

# DIVERGENCE-FREE WAVELET PROJECTION METHOD FOR INCOMPRESSIBLE VISCOUS FLOW

SOULEYMANE KADRI HAROUNA\* AND VALÉRIE PERRIER†

**Abstract.** We present a new wavelet numerical scheme for the discretization of Navier-Stokes equations with physical boundary conditions. The temporal discretization of the method is inspired from the projection method. Classical Helmholtz-Hodge decomposition using appropriate divergence-free and curl-free wavelet bases allows to define the projection operator and to reduce the steps of usual methods with more accuracy. Numerical experiments conducted on the simulation of lid driven cavity flow with high Reynolds number show the validity and the precision of the method. Divergence-free wavelet numerical adaptativity is proved.

**Key words.** Divergence-free wavelets, Navier-Stokes simulation, physical boundary conditions

**1. Introduction.** The characterization of turbulent flows is a continuing challenge encountered in several scientific areas. Physically, turbulent flows are characterized by the presence of many phenomena at different scales in interaction and with rapid variations in time and space. The mathematical equations that model turbulent flows are the Navier-Stokes equations, which are derived from newtonian laws in the context of hydrodynamics [29]:

$$\begin{cases} \mathbf{v}_t - \nu \Delta \mathbf{v} + (\mathbf{v} \cdot \nabla) \mathbf{v} + \nabla p = 0 \\ \nabla \cdot \mathbf{v} = 0 \end{cases} \quad (1.1)$$

on  $\Omega \subset \mathbb{R}^d$ , where  $\mathbf{v} \in \mathbb{R}^d$  denotes the velocity vector field,  $p \in \mathbb{R}$  is the pressure and  $\nu > 0$  is the kinematic viscosity. We focus in this paper on the two-dimensional equations ( $d = 2$ ), the extension of our method to the dimension three being straightforward.

To take into account the physic of the problem, we suppose that the fluid is confined in  $\Omega$ , so it does not cross the boundary  $\Gamma = \partial\Omega$ . In this case, the velocity field  $\mathbf{v}$  must be tangential to the boundary:

$$\mathbf{v} \cdot \mathbf{n} = 0 \quad \text{on } \Gamma. \quad (1.2)$$

The viscous friction of the fluid particles leads to no slip on the boundary  $\Gamma$ :

$$\mathbf{v} = 0 \quad \text{on } \Gamma. \quad (1.3)$$

One can also study a particular region of the fluid, so it is not confined in  $\Omega$ : the fluid can pass through  $\Gamma$ . In this case, we suppose known the velocity  $\mathbf{v}$  on the boundary:

$$\mathbf{v} = g \quad \text{on } \Gamma, \quad (1.4)$$

with  $\int_{\Gamma} g \cdot \mathbf{n} ds = 0$  to satisfy the incompressibility constraint.

---

\*INRIA, Fluminance group, Campus universitaire de Beaulieu, 35042 Rennes, France ([souleymane.kadri\\_harouna@inria.fr](mailto:souleymane.kadri_harouna@inria.fr)).

†Laboratoire Jean-Kunztmann, Université de Grenoble, CNRS, 38041 Grenoble Cedex 9, France ([valerie.perrier@imag.fr](mailto:valerie.perrier@imag.fr)).

Then, the construction of performing numerical schemes is very important for effective models of prediction.

The difficulty in the numerical resolution of Navier-Stokes equations comes from the nature of equations which are nonlinear. The interest of the velocity-pressure formulation is that physical boundary condition on  $\mathbf{v}$  (1.2, 1.3 or 1.4) can be simply imposed into the numerical approximation. The projection method has for advantage to decouple the computation of the velocity  $\mathbf{v}$  and the pressure  $p$  [7, 28].

To incorporate the incompressibility constraint and the previous boundary conditions, let us introduce the divergence-free function space, with free-slip boundary condition:

$$\mathcal{H}_{div}(\Omega) = \{\mathbf{u} \in (L^2(\Omega))^2 : \nabla \cdot \mathbf{u} = 0, \mathbf{u} \cdot \mathbf{n}|_{\Gamma} = 0\}. \quad (1.5)$$

By Stokes theorem, the space  $\mathcal{H}_{div}(\Omega)$  is orthogonal to any gradient in  $(L^2(\Omega))^2$  [18]. Then, projecting the Navier-Stokes equations (1.1) onto  $\mathcal{H}_{div}(\Omega)$  yields:

$$\begin{cases} \mathbf{v}_t + \mathbb{P}[-\nu\Delta\mathbf{v} + (\mathbf{v} \cdot \nabla)\mathbf{v}] = 0, & \text{on } \Omega \\ \nabla \cdot \mathbf{v} = 0 \end{cases} \quad (1.6)$$

where  $\mathbb{P}$  denotes the orthogonal projector from  $(L^2(\Omega))^2$  to  $\mathcal{H}_{div}(\Omega)$ . According to the Helmholtz-Hodge decomposition, the pressure verifies the following equation:

$$\nabla p = -\nu\Delta\mathbf{v} + (\mathbf{v} \cdot \nabla)\mathbf{v} - \mathbb{P}[-\nu\Delta\mathbf{v} + (\mathbf{v} \cdot \nabla)\mathbf{v}]. \quad (1.7)$$

Now the difficulty relies on the integration in time of (1.6). The conventional projection method consists in a splitting of this operator:  $\mathbf{v}_t - \nu\mathbb{P}\Delta\mathbf{v}$ .

In the simplest case of periodic boundary conditions, the first equation of (1.6) becomes:

$$\mathbf{v}_t - \nu\Delta\mathbf{v} + \mathbb{P}[(\mathbf{v} \cdot \nabla)\mathbf{v}] = 0, \quad (1.8)$$

and the pressure  $p$  is recovered via:

$$\nabla p = \mathbf{v} - \mathbb{P}[(\mathbf{v} \cdot \nabla)\mathbf{v}] \quad (1.9)$$

This formulation was used by [13, 14] to derive a divergence-free wavelet resolution method. One can remark that this approach is very close to the projection method, since the numerical resolution of (1.8) reduces to a heat kernels integration with source term as the projection onto divergence-free function space of the nonlinear term  $\mathbb{P}[(\mathbf{v} \cdot \nabla)\mathbf{v}]$ . Using (for example) a backward Euler schemes in time, the method of [13, 14] is summarized as follows: starting with  $\mathbf{v}^n$ , compute  $\mathbf{v}^{n+1}$  by

$$\mathbf{v}^{n+1} - \mathbf{v}^n - \delta t\nu\Delta\mathbf{v}^{n+1} + \delta t\mathbb{P}[(\mathbf{v}^n \cdot \nabla)\mathbf{v}^n] = 0, \quad (1.10)$$

where the term  $(\mathbf{v}^n \cdot \nabla)\mathbf{v}^n$  is computed explicitly on the mesh grid points. Each time step requires the computation of projector  $\mathbb{P}$ , which is done using an iterative algorithm of [12]. The method gives rise to sparse representation of the velocity and coherent structures of the flow, and adaptive discretizations can be derived easily.

Our objective in the next coming sections is to provide an effective numerical method similar to (1.10), more flexible for desired boundary conditions and easy to implement.

In the case of physical boundary conditions (1.2), (1.3) and (1.4) the situation becomes more complicated. The projector  $\mathbb{P}$  does not more commute with the Laplacian operator:

$$\mathbb{P}(\Delta \mathbf{v}) \neq \Delta \mathbb{P}(\mathbf{v}). \quad (1.11)$$

Taking the divergence of (1.7), we see that  $p$  is linked to the non-linear term  $(\mathbf{v} \cdot \nabla) \mathbf{v}$  by:

$$\Delta p = \nabla \cdot [(\mathbf{v} \cdot \nabla) \mathbf{v}]. \quad (1.12)$$

The resulting equations (1.6), (1.9), (1.7) and (1.12) can be solved by standard methods for heat and Poisson equation, for which a large number of works exist [18, 29].

From another point of view, the construction of divergence-free wavelet bases on square /cubic domains satisfying physical boundary conditions [24, 26, 27], allows to explicitly compute the Helmholtz-Hodge decomposition in wavelet domain [25]. Based on this new numerical issue to compute the projector  $\mathbb{P}$ , we present a new formulation of the projection method for Navier-Stokes equations [1, 7, 20, 28]. The method we develop in this article will not use a Poisson solver as in usual methods.

The layout of the paper is as follows. In Section 2 we recall the setting of divergence-free wavelet bases on the square satisfying boundary conditions, and the computation of the Leray-Hopf projector  $\mathbb{P}$ . In Section 3 we present the classical divergence-free wavelets schemes for the Stokes equations and we use the ingredients of previous sections to derive a new projection method for Navier-Stokes equations based on divergence-free wavelets. Section 4 presents numerical results that valid our method.

**2. Divergence-free and Curl-free Wavelets on  $[0, 1]^2$ .** This section introduces the principles of the construction and main properties of divergence-free and curl-free wavelets bases. The construction will be provided on the square  $[0, 1]^2$  and for more details see [25].

**2.1. Divergence-free and Curl-free Wavelets .** Since the seminal works of Lemarié-Rieusset and collaborators [19, 21], the construction of divergence-free and curl-free wavelets is based on one-dimensional multiresolution analyses linked by differentiation / integration. It follows two principle steps:

(i) Construct two biorthogonal multiresolution analyses of  $L^2(0, 1)$  denoted  $(V_j^1, \tilde{V}_j^1)$  and  $(V_j^0, \tilde{V}_j^0)$  satisfying:

$$\frac{d}{dx} V_j^1 = V_j^0 \quad \text{and} \quad \tilde{V}_j^0 = \left\{ \int_0^x f(t) dt : f \in \tilde{V}_j^1 \right\} \cap H_0^1(0, 1). \quad (2.1)$$

Each space is spanned by scaling functions

$$V_j^1 = \text{span}\{\varphi_{j,k}^1 ; 0 \leq k \leq N_j - 1\} \quad \text{and} \quad \tilde{V}_j^1 = \text{span}\{\tilde{\varphi}_{j,k}^1 ; 0 \leq k \leq N_j - 1\}, \quad (2.2)$$

and

$$V_j^0 = \text{span}\{\varphi_{j,k}^0 ; 0 \leq k \leq N_j - 2\} \quad \text{and} \quad \tilde{V}_j^0 = \text{span}\{\tilde{\varphi}_{j,k}^0 ; 0 \leq k \leq N_j - 2\}, \quad (2.3)$$

whose dimension  $N_j \simeq 2^j$  depends on some *free* integer parameters  $(\delta_0, \delta_1)$ . The scaling functions  $\varphi_{j,k}^1$  satisfy  $\varphi_{j,k}^1 = 2^{j/2}\varphi^1(2^j x - k)$  inside the interval  $[0, 1]$ , but this is no more true near the boundaries 0 and 1 (idem for  $\tilde{\varphi}_{j,k}^1$ ). In practice, the scale index  $j$  must be great than some index  $j_{min}$ , to avoid boundary effects [23]. The biorthogonality between bases writes:  $\langle \varphi_{j,k}^1 / \tilde{\varphi}_{j,k'}^1 \rangle = \delta_{k,k'}$ .

Biorthogonal wavelets are bases of the complement spaces of  $(V_j^1, \tilde{V}_j^1)$ , denoted  $(W_j^1, \tilde{W}_j^1)$ :

$$W_j^1 = V_{j+1}^1 \cap (\tilde{V}_j^1)^\perp \quad \tilde{W}_j^1 = \tilde{V}_{j+1}^1 \cap (V_j^1)^\perp. \quad (2.4)$$

These spaces are generated by finite dimensional biorthogonal wavelet bases on the interval [23]:

$$W_j^1 = \text{span}\{\psi_{j,k}^1 ; 0 \leq k \leq 2^j - 1\} \quad \text{and} \quad \tilde{W}_j^1 = \text{span}\{\tilde{\psi}_{j,k}^1 ; 0 \leq k \leq 2^j - 1\} \quad (2.5)$$

Biorthogonal wavelet bases of  $W_j^0 = \text{span}\{\psi_{j,k}^0\}_{j \geq j_{min}}$  and  $\tilde{W}_j^0 = \text{span}\{\tilde{\psi}_{j,k}^0\}_{j \geq j_{min}}$  are simply defined by respectively differentiating and integrating the wavelets bases of  $(W_j^1, \tilde{W}_j^1)_{j \geq j_{min}}$  [19, 26]:

$$\psi_{j,k}^0 = 2^{-j}(\psi_{j,k}^1)' \quad \text{and} \quad \tilde{\psi}_{j,k}^0 = -2^j \int_0^x \tilde{\psi}_{j,k}^1 \quad (2.6)$$

Homogeneous Dirichlet boundary conditions can be simply imposed on  $(V_j^1, \tilde{V}_j^1)$  by removing scaling functions that reproduce constant at each boundary 0 and 1, prior biorthogonalization [23]. Then, the spaces

$$V_j^d = V_j^1 \cap H_0^1(0, 1) = \text{span}\{\varphi_{j,k}^1 ; 1 \leq k \leq N_j - 2\} \quad (2.7)$$

and

$$\tilde{V}_j^d = \tilde{V}_j^1 \cap H_0^1(0, 1) = \text{span}\{\tilde{\varphi}_{j,k}^1 ; 1 \leq k \leq N_j - 2\} \quad (2.8)$$

provide biorthogonal multiresolution analyses for  $H_0^1(0, 1)$  [9, 10, 23].

### (ii) Divergence-free and Curl-free Wavelets Construction

Following (1.5),  $\mathcal{H}_{div}(\Omega)$  is the curl of  $H_0^1(\Omega)$  stream functions and  $\mathcal{H}_{curl}(\Omega)$  is the gradient of  $H_0^1(\Omega)$  potentials:

$$\mathcal{H}_{div}(\Omega) = \{\mathbf{u} = \mathbf{curl}(\Psi) : \Psi \in H_0^1(\Omega)\} \quad (2.9)$$

and

$$\mathcal{H}_{curl}(\Omega) = \{\mathbf{u} = \nabla q : q \in H_0^1(\Omega)\}. \quad (2.10)$$

Since the spaces  $(V_j^d \otimes V_j^d)_{j \geq j_{min}}$  provide a MRA of  $H_0^1(\Omega)$  (2.8), divergence-free and curl-free scaling functions on  $\Omega = [0, 1]^2$  are constructed by taking the curl of and the gradient of scaling functions of  $V_j^d \otimes V_j^d$  respectively:

$$\Phi_{\mathbf{j}, \mathbf{k}}^{div} := \mathbf{curl}[\varphi_{j,k_1}^d \otimes \varphi_{j,k_2}^d] = \begin{cases} \varphi_{j,k_1}^d \otimes (\varphi_{j,k_2}^d)' \\ -(\varphi_{j,k_1}^d)' \otimes \varphi_{j,k_2}^d \end{cases}, \quad 1 \leq k_1, k_2 \leq N_j - 2 \quad (2.11)$$

and

$$\Phi_{\mathbf{j}, \mathbf{k}}^{curl} := \mathbf{grad}[\varphi_{j,k_1}^d \otimes \varphi_{j,k_2}^d] = \begin{cases} (\varphi_{j,k_1}^d)' \otimes \varphi_{j,k_2}^d \\ \varphi_{j,k_1}^d \otimes (\varphi_{j,k_2}^d)' \end{cases}, \quad 1 \leq k_1, k_2 \leq N_j - 2 \quad (2.12)$$

The choice of spaces  $V_j^d$  ensures the orthogonality between scaling functions  $\Phi_{\mathbf{j}, \mathbf{k}}^{div}$  and  $\Phi_{\mathbf{j}, \mathbf{k}}^{curl}$ . Moreover, boundary conditions are satisfied by construction.

Let  $\{\psi_{j,k}^d\}$  be the wavelet basis of  $W_j^d = V_{j+1}^d \cap (\tilde{V}_j^d)^\perp$ . Accordingly, anisotropic divergence-free and curl-free wavelets on  $[0, 1]^2$  are constructed by taking respectively the curl and the gradient of the three types of scalar anisotropic wavelets associated to  $V_j^d \otimes V_j^d$ :

$$\Psi_{\mathbf{j}, \mathbf{k}}^{div,1} := \mathbf{curl}[\varphi_{j_{min},k}^d \otimes \psi_{j_2,k_2}^d] \quad \text{and} \quad \Psi_{\mathbf{j}, \mathbf{k}}^{curl,1} := \nabla[\varphi_{j_{min},k}^d \otimes \psi_{j_2,k_2}^d],$$

$$\Psi_{\mathbf{j}, \mathbf{k}}^{div,2} := \mathbf{curl}[\psi_{j_1,k_1}^d \otimes \varphi_{j_{min},k}^d] \quad \text{and} \quad \Psi_{\mathbf{j}, \mathbf{k}}^{curl,2} := \nabla[\psi_{j_1,k_1}^d \otimes \varphi_{j_{min},k}^d],$$

$$\Psi_{\mathbf{j}, \mathbf{k}}^{div,3} := \mathbf{curl}[\psi_{j_1,k_1}^d \otimes \psi_{j_2,k_2}^d] \quad \text{and} \quad \Psi_{\mathbf{j}, \mathbf{k}}^{curl,3} := \nabla[\psi_{j_1,k_1}^d \otimes \psi_{j_2,k_2}^d].$$

**2.2. Leray-Hopf Projector Computation .** In this section we introduce briefly some settings and definitions to compute in practice the Leray-Hopf projector  $\mathbb{P}$ , using divergence-free wavelet bases.

The divergence-free wavelet basis constructed in Section 2 provides an alternative wavelet basis for  $\mathcal{H}_{div}(\Omega)$ :

$$\mathcal{H}_{div}(\Omega) = \text{span}\{\Psi_{\mathbf{j}, \mathbf{k}}^{div}\}, \quad \forall \mathbf{j}, \mathbf{k}, \quad \nabla \cdot \Psi_{\mathbf{j}, \mathbf{k}}^{div} = 0 \quad \text{and} \quad \Psi_{\mathbf{j}, \mathbf{k}}^{div} \cdot \mathbf{n} = 0. \quad (2.13)$$

The Helmholtz-Hodge decomposition theorem states that for any vector field  $\mathbf{u} \in L^2(\Omega)^2$ , there exist unique  $q \in H^1(\Omega)$  with  $\int_\Omega q = 0$ , such that:

$$\mathbf{u} = \mathbf{u}_{div} + \nabla q \quad \text{and} \quad \mathbb{P}(\mathbf{u}) = \mathbf{u}_{div}. \quad (2.14)$$

Searching  $\mathbf{u}_{div}$  in terms of its divergence-free wavelet series

$$\mathbf{u}_{div} = \sum_{\mathbf{j}, \mathbf{k}} d_{\mathbf{j}, \mathbf{k}}^{div} \Psi_{\mathbf{j}, \mathbf{k}}^{div}, \quad (2.15)$$

and by the orthogonality  $\Psi_{\mathbf{j}, \mathbf{k}}^{div} \perp \nabla q$  in  $(L^2(\Omega))^2$ , we obtain:

$$\langle \mathbf{u}, \Psi_{\mathbf{j}, \mathbf{k}}^{div} \rangle = \langle \mathbf{u}_{div}, \Psi_{\mathbf{j}, \mathbf{k}}^{div} \rangle. \quad (2.16)$$

Accordingly the computation of coefficients  $(d_{\mathbf{j},\mathbf{k}}^{\text{div}})$  is reduced to the resolution of a linear systems:

$$\mathbb{M}_{\text{div}}(d_{\mathbf{j},\mathbf{k}}^{\text{div}}) = (\langle \mathbf{u}, \Psi_{\mathbf{j},\mathbf{k}}^{\text{div}} \rangle) \quad (2.17)$$

where  $\mathbb{M}_{\text{div}}$  denotes the Gram matrix of the basis  $\{\Psi_{\mathbf{j},\mathbf{k}}^{\text{div}}\}$  and the computation of its elements and the right term  $(\langle \mathbf{u}, \Psi_{\mathbf{j},\mathbf{k}}^{\text{div}} \rangle)$  in (2.17) are done following [25]. Since in dimension  $d = 2$ , the  $\Psi_{\mathbf{j},\mathbf{k}}^{\text{div}}$  are "curl" functions, the matrix  $\mathbb{M}_{\text{div}}$  is no more than the matrix of the 2D Laplacian operator on the wavelet basis associated to the multiresolution analysis  $(V_j^d \otimes V_j^d)$  of  $H_0^1(\Omega)$ . Following [8], we showed in [25] that its diagonal is an optimal preconditioner. The tensor structure of the basis allows to reduce the complexity of matrix-vector product  $\mathbb{M}_{\text{div}}(d_{\mathbf{j},\mathbf{k}}^{\text{div}})$ . If  $J$  is the maximal one dimension space resolution *i.e*  $N_J - 2 \simeq 2^J$ , the theoretical complexity of the inversion of system (2.17) with a preconditioned conjugate gradient method is about  $O(2^{3J})$ , see [25] for details.

**3. A New Projection Method by Divergence-free Wavelets.** The purpose in this section is to introduce a new formulation of time discretization of the instationary Stokes and Navier-Stokes equations, for incompressible viscous flows. The method can be seen as a variant of the projection method [1, 7, 20, 28], where we have replaced the operator splitting by the exact Helmholtz-Hodge decomposition of the intermediate velocity field. The method allows to compute the exact velocity field from the intermediate one by using only boundary condition satisfied by this velocity field. Then, we prevent some numerical difficulties and drawbacks related to the computation of the pressure at each time step with artificial boundary conditions done in the classical approaches [1, 20].

**3.1. General Principles of Divergence-free Wavelet Schemes for the Stokes Equations.** The use of divergence-free wavelet bases in the numerical simulation of turbulent flow began with the works of Urban [11, 30], for the resolution of stationary Stokes problem:

$$\begin{cases} -\nu \Delta \mathbf{v} + \nabla p = \mathbf{f}, \\ \nabla \cdot \mathbf{v} = 0, \end{cases} \quad (3.1)$$

in  $\Omega = [0, 1]^2$ , with periodic or homogeneous Dirichlet boundary conditions.

The main advantage of using divergence-free wavelet basis in the resolution of Stokes equations is the direct representation of the incompressibility constraint of the flow. To solve (3.1), as in the Urban's works [30, 31] variational approach with a Galerkin type approximation can be used. In this case, the velocity field  $\mathbf{v}$  is searched in terms of its divergence-free wavelet coefficients:

$$\mathbf{v}(x) = \sum_{\mathbf{j},\mathbf{k}} d_{\mathbf{j},\mathbf{k}} \Psi_{\mathbf{j},\mathbf{k}}^{\text{div}}(x). \quad (3.2)$$

Replacing (3.2) in (3.1), the computation of coefficients  $d_{\mathbf{j},\mathbf{k}}$  is done by solving a linear system with the stiffness matrix of divergence-free wavelet basis:

$$\sum_{\mathbf{j},\mathbf{k}} d_{\mathbf{j},\mathbf{k}} \langle \nu \nabla \Psi_{\mathbf{j},\mathbf{k}}^{\text{div}}, \nabla \Psi_{\mathbf{j}',\mathbf{k}'}^{\text{div}} \rangle = \langle \mathbf{f}, \Psi_{\mathbf{j}',\mathbf{k}'}^{\text{div}} \rangle, \quad \forall \mathbf{j}', \mathbf{k}'. \quad (3.3)$$

The matrix of terms  $\langle \nu \nabla \Psi_{\mathbf{j}, \mathbf{k}}^{div}, \nabla \Psi_{\mathbf{j}', \mathbf{k}'}^{div} \rangle$  is symmetric and the associated bilinear form is coercive [30]. The problem is thus reduced to an elliptic problem on the divergence-free function space and standard estimations on the truncature error and on the regularity of the solution can be derived. In addition, the formulation (3.3) has the advantage to eliminate directly the pressure  $p$  which is computed by a post processing procedure [30].

In comparison with classical approaches based on finite differences, finite elements or wavelet method [5, 18], equation (3.3) has the advantage of reducing the number of degree of freedom: only coefficients  $\{d_{\mathbf{j}, \mathbf{k}}\}$  are computed instead of one type of coefficients per components of the velocity  $\mathbf{v}$ . Moreover, adaptive methods can be applied and optimal preconditioning for the stiffness matrix can be provided explicitly. However, for homogeneous Dirichlet boundary condition, the method was less effective in the approximation at the edges and preconditioning becomes a problem in three dimension for example. Since the homogeneous divergence-free wavelets construction of [30] uses only trial functions that have their support strictly inside of  $\Omega$ , the loss of precision at boundaries creates numerical instabilities.

For the instationary problem, recently Stevenson [27] has proposed a new theoretical variational formulation of the Stokes equations. The method of Stevenson is an extension of Urban's method to the instationary problem and use divergence-free wavelets satisfying a free-slip boundary condition. However, unhomogeneous boundary conditions can not be considered easily in these methods.

Contrarily to Urban and Stevenson works, our objective in next coming sections consists on developing a method that uses Galerkin variational formulation with standard wavelet basis and the Leray-Hopf projector  $\mathbb{P}$ . Especially to construct a new projection method using divergence-free wavelets satisfying the free-slip boundary condition. The advantage is that classical wavelet method can be used to solve the diffusion problem and the incompressibility constraint is incorporated via the projector  $\mathbb{P}$ . The approach includes one phase devoted to the temporal discretization and a second one of spacial discretization.

**3.1.1. A New Projection Method for the unstationary Stokes equations.** We consider in this section the unstationary Stokes problem, with no-sleep boundary conditions:

$$\begin{cases} \partial_t \mathbf{v} - \nu \Delta \mathbf{v} + \nabla p = \mathbf{f}, \\ \mathbf{v} = 0 \text{ on } \partial\Omega, \\ \nabla \cdot \mathbf{v} = 0. \end{cases} \quad (3.4)$$

For the temporal discretization of equations (3.4) we use finite difference method. Given a time step  $\delta t$  and considering the approximation  $\mathbf{v}^n(x) \approx \mathbf{v}(x, n\delta t)$ , using a backward Euler scheme we get:

$$\frac{\mathbf{v}^{n+1} - \mathbf{v}^n}{\delta t} - \nu \Delta \mathbf{v}^{n+1} + \nabla p^{n+1} = \mathbf{f}^n, \quad \nabla \cdot \mathbf{v}^{n+1} = 0. \quad (3.5)$$

However, scheme (3.5) is inefficient since it requires, at each time step, the evaluation of coupled equations for  $(\mathbf{v}^{n+1}, p^{n+1})$ .

Now, let us introduce a new variable  $\tilde{\mathbf{v}}$  by setting  $\tilde{\mathbf{v}} = \mathbf{v}^{n+1} + \nabla\Phi^{n+1}$ , one can prove that  $\tilde{\mathbf{v}}$  verifies the following system:

$$\frac{\tilde{\mathbf{v}} - \mathbf{v}^n}{\delta t} - \nu\Delta\tilde{\mathbf{v}} + \nabla[p^{n+1} - \frac{1}{\delta t}\Phi^{n+1} + \nu\Delta\Phi^{n+1}] = \mathbf{f}^n, \quad \mathbf{v}^{n+1} = \mathbb{P}(\tilde{\mathbf{v}}). \quad (3.6)$$

If the pressure  $p^{n+1}$  is defined as:

$$p^{n+1} - \frac{1}{\delta t}\Phi^{n+1} + \nu\Delta\Phi^{n+1} = 0, \quad (3.7)$$

the system of equations (3.6) reduces to

$$\frac{\tilde{\mathbf{v}} - \mathbf{v}^n}{\delta t} - \nu\Delta\tilde{\mathbf{v}} = \mathbf{f}^n, \quad \mathbf{v}^{n+1} = \mathbb{P}(\tilde{\mathbf{v}}). \quad (3.8)$$

This equation requires the resolution of a heat equation and the projection (Section 2.2). For the spacial approximation, a variational Galerkin method is used on a suitable ensorial wavelet basis.

**3.1.2. Spatial discretization of Stokes equations.** For the spatial discretization, we use the multiresolution analysis of  $(L^2(\Omega))^d$  that contains the divergence-free wavelets. In two space dimension, this multiresolution analysis is constituted by the spaces  $\mathbf{V}_j = (V_j^1 \otimes V_j^0) \times (V_j^0 \otimes V_j^1)$ . Then, at a given resolution  $j$ , the components of  $\mathbf{v}^n = (v_1^n, v_2^n)$  are searched under the form of a finite dimensional wavelet series:

$$v_1^n = \sum_{|\mathbf{j}| < j, \mathbf{k}} d_{\mathbf{j}, \mathbf{k}}^1 \psi_{j_1, k_1}^1 \otimes \psi_{j_2, k_2}^0 \quad \text{and} \quad v_2^n = \sum_{|\mathbf{j}| < j, \mathbf{k}} d_{\mathbf{j}, \mathbf{k}}^2 \psi_{j_1, k_1}^0 \otimes \psi_{j_2, k_2}^1, \quad (3.9)$$

and similarly for  $\tilde{\mathbf{v}}$  with coefficients  $[\tilde{d}_{\mathbf{j}, \mathbf{k}}^1]$  and  $[\tilde{d}_{\mathbf{j}, \mathbf{k}}^2]$ . The computation of the invert of the matrix of operator  $(1 - \delta t \nu \Delta)$  at each time step and this is as follows: we use the method of [6], consisting on the factorization of heat operator kernel, remaining in the context of alternated direction implicit methods. Precisely, for small  $\alpha$ , in two dimension we have:

$$(1 - \alpha\Delta) \approx (1 - \alpha\frac{\partial^2}{\partial x^2})(1 - \alpha\frac{\partial^2}{\partial y^2}). \quad (3.10)$$

Thus, in (3.8) we have only to invert the matrix of one-dimensional heat operator  $(1 - \delta t \nu \frac{\partial^2}{\partial x^2})$ , and this is done once before to start the time integration procedure. Ultimately, the computation of coefficients  $[\tilde{d}_{\mathbf{j}, \mathbf{k}}^1]$  and  $[\tilde{d}_{\mathbf{j}, \mathbf{k}}^2]$  from those of  $\mathbf{v}^n(x)$  is reduced to solving a matrices linear system:

$$\mathcal{A}_{\delta t}^1[\tilde{d}_{\mathbf{j}, \mathbf{k}}^{1, n}] \mathcal{A}_{\delta t}^0 = \mathcal{M}^1[d_{\mathbf{j}, \mathbf{k}}^{1, n}] \mathcal{M}^0 + \delta t \mathcal{M}^1 \mathbf{f}_1^n \mathcal{M}^0 \quad (3.11)$$

and

$$\mathcal{A}_{\delta t}^0[\tilde{d}_{\mathbf{j}, \mathbf{k}}^{2, n}] \mathcal{A}_{\delta t}^1 = \mathcal{M}^0[d_{\mathbf{j}, \mathbf{k}}^{2, n}] \mathcal{M}^1 + \delta t \mathcal{M}^0 \mathbf{f}_2^n \mathcal{M}^1, \quad (3.12)$$

where  $\mathcal{A}_{\delta t}^i$  and  $\mathcal{M}^i$  correspond to stiffness matrix of operator  $(1 - \delta t \nu \frac{\partial^2}{\partial x^2})$  and mass matrix on the one-dimensional wavelet bases of  $\{V_j^i\}_{i=0,1}$ . The elements of these matrices are computed analytically by solving an eigenvalue problem [2].



In summary, the algorithm of resolution is the following. Starting with an initial value  $\tilde{\mathbf{v}}_0(x) = \mathbf{v}_0(x) = \mathbf{v}(0, x)$ , compute its coefficients  $[d_{\mathbf{j}, \mathbf{k}}^{1,0}]$  and  $[d_{\mathbf{j}, \mathbf{k}}^{2,0}]$  on  $\mathbf{V}_j = (V_j^1 \otimes V_j^0) \times (V_j^0 \otimes V_j^1)$  by an interpolation procedure [24]. For  $1 \leq n \leq N$ , repeat

**Step 1:** Find  $[d_{\mathbf{j}, \mathbf{k}}^{1,n}]$  and  $[d_{\mathbf{j}, \mathbf{k}}^{2,n}]$  solution of

$$\mathcal{A}_{\delta t}^1 [d_{\mathbf{j}, \mathbf{k}}^{1,n}] \mathcal{A}_{\delta t}^0 = \mathcal{M}^1 [d_{\mathbf{j}, \mathbf{k}}^{1,n}] \mathcal{M}^0 + \delta t \mathcal{M}^1 \mathbf{f}_1^n \mathcal{M}^0$$

$$\mathcal{A}_{\delta t}^0 [d_{\mathbf{j}, \mathbf{k}}^{2,n}] \mathcal{A}_{\delta t}^1 = \mathcal{M}^0 [d_{\mathbf{j}, \mathbf{k}}^{2,n}] \mathcal{M}^1 + \delta t \mathcal{M}^0 \mathbf{f}_2^n \mathcal{M}^1$$

**Step 2:** Find  $[\mathbf{d}_{\mathbf{j}, \mathbf{k}}^{div, n+1}]$  solution of

$$\mathcal{M}^1 [d_{\mathbf{j}, \mathbf{k}}^{1,n}] \mathcal{A}_d^0 - (\mathcal{A}_d^0)^T [d_{\mathbf{j}, \mathbf{k}}^{2,n}] \mathcal{M}^1 = \mathcal{M}^1 [d_{\mathbf{j}, \mathbf{k}}^{div, n+1}] \mathcal{R}^1 + \mathcal{R}^1 [d_{\mathbf{j}, \mathbf{k}}^{div, n+1}] \mathcal{M}^1$$

where  $\mathcal{R}^1$  is the stiffness matrix of wavelet basis  $\{\psi_{j,k}^d\}$ , its terms correspond to  $\langle (\psi_{j,k}^d)' , (\psi_{j',k'}^d)' \rangle$  and the terms of  $\mathcal{A}_d^0$  correspond to  $\langle \psi_{j,k}^0, (\psi_{j',k'}^d)' \rangle$ .

**Step 3:** Compute  $[d_{\mathbf{j}, \mathbf{k}}^{1, n+1}]$  and  $[d_{\mathbf{j}, \mathbf{k}}^{2, n+1}]$  from  $[\mathbf{d}_{\mathbf{j}, \mathbf{k}}^{div, n+1}]$  using the change of basis between  $\{(\psi_{j,k}^1)'\}$  and  $\{\psi_{j,k}^0\}$ .

As the matrices  $\mathcal{A}_{\delta t}^1$  and  $\mathcal{A}_{\delta t}^0$  are inverted once before starting the algorithm, Step 1 is thus only a matrix multiplication. If  $J$  denotes the maximal space resolution, the theoretical complexity of this step is  $O(2^{3J})$ . Step 2 correspond to  $\mathbf{v}^{n+1} = \mathbb{P}(\tilde{\mathbf{v}})$  and it is solved with a preconditioned conjugate gradient method, then its theoretical complexity is  $O(2^{3J})$ . The last step is a change of basis, which complexity is linear. We deduce that the theoretical complexity of the method is about  $O(2^{3J})$ .

**3.1.3. Stability and consistency analysis.** The main concerns in this section is to analyze the stability and consistency of the introduced modified projection method for the Stokes problem. For sake of simplicity we take  $\mathbf{f}^n = 0$  in (3.8) and suppose that is *regular* and  $\mathbf{v}^n \in L^2(\Omega)^d$ .

To prove the stability of our schemes, standard energy estimate will be used with  $\tilde{\mathbf{v}}$  as test function, thanks to the boundary conditions on  $\tilde{\mathbf{v}}$ . Taking the inner product of equation (3.8) with  $2\tilde{\mathbf{v}}$ , we have

$$\|\tilde{\mathbf{v}}\|_{L^2}^2 + \|\tilde{\mathbf{v}} - \mathbf{v}^n\|_{L^2}^2 - \|\mathbf{v}^n\|_{L^2}^2 + 2\nu\delta t \|\nabla \tilde{\mathbf{v}}\|_{L^2}^2 = 0. \quad (3.13)$$

Since  $\tilde{\mathbf{v}} = \mathbf{v}^{n+1} + \nabla \phi^{n+1}$ , which is an orthogonal decomposition in  $L^2(\Omega)^d$ , equation (3.13) is simplified as

$$\|\mathbf{v}^{n+1}\|_{L^2}^2 + \|\mathbf{v}^{n+1} - \mathbf{v}^n\|_{L^2}^2 + 2\|\nabla \phi^{n+1}\|_{L^2}^2 - \|\mathbf{v}^n\|_{L^2}^2 + 2\nu\delta t \|\nabla \tilde{\mathbf{v}}\|_{L^2}^2 = 0. \quad (3.14)$$

Then the modified projection method (3.7) and (3.8) is unconditionally stable for the Stokes equations.

The consistency of the method is a consequence of the following theorem

**THEOREM 3.1.** *Let  $\mathbf{v}$  be a smooth function solution of Stokes equations with smooth initial data  $\mathbf{v}_0(x)$  and let  $\mathbf{v}_{\delta t}$  be the numerical solution of the semi-discrete modified projection method (3.7) and (3.8), then:*

$$\|\mathbf{v} - \mathbf{v}_{\delta t}\|_{L^\infty([0,T];L^2)} \leq C_1 \delta t, \quad (3.15)$$

$$\|\nabla \mathbf{v} - \nabla \mathbf{v}_{\delta t}\|_{L^\infty([0,T];L^2)} \leq C_2 \delta t^{1/2}. \quad (3.16)$$

*Proof.* Let  $\mathbf{v}^{n+1}$  be the solution of (3.7) and (3.8) computed from  $\mathbf{v}^n = \mathbf{v}(x, n\delta t)$ . Let  $\epsilon^{n+1} = \mathbf{v}(x, n\delta t + \delta t) - \mathbf{v}^{n+1}$  be the consistency error. Thus, the error  $\epsilon^{n+1}$  is linked to  $\tilde{\mathbf{v}}$  by:

$$\tilde{\mathbf{v}} = \mathbf{v}(x, n\delta t + \delta t) + \nabla \Phi^{n+1} - \epsilon^{n+1}. \quad (3.17)$$

Replacing (3.17) in (3.7) and with (3.8), we get:

$$-\epsilon^{n+1} + \nu \delta t \Delta \epsilon^{n+1} + \delta t \nabla p^{n+1} + \mathbf{v}(x, n\delta t + \delta t) - \mathbf{v}^n - \nu \delta t \Delta \mathbf{v}(x, n\delta t + \delta t) = 0. \quad (3.18)$$

Using the Taylor serie approximation:

$$\mathbf{v}(x, n\delta t + \delta t) = \mathbf{v}^n + \delta t \partial_t \mathbf{v}(x, n\delta t) + O(\delta t^2), \quad (3.19)$$

the terms  $\mathbf{v}(x, n\delta t + \delta t) - \mathbf{v}^n - \nu \delta t \Delta \mathbf{v}(x, n\delta t + \delta t)$  of (3.18) are simplified as:

$$\mathbf{v}(x, n\delta t + \delta t) - \mathbf{v}^n - \nu \delta t \Delta \mathbf{v}(x, n\delta t + \delta t) = \delta t [\partial_t \mathbf{v}(x, n\delta t) - \nu \Delta \mathbf{v}(x, n\delta t)] + O(\delta t^2).$$

Since  $\partial_t \mathbf{v}(x, n\delta t) - \nu \Delta \mathbf{v}(x, n\delta t) = -\nabla p(x, n\delta t)$ , equation (3.18) rewritten as:

$$-\epsilon^{n+1} + \nu \delta t \Delta \epsilon^{n+1} = \delta t \nabla [p(x, n\delta t) - p^{n+1}] + O(\delta t^2). \quad (3.20)$$

By definition,  $\epsilon^{n+1}$  is divergence-free:  $\nabla \cdot \epsilon^{n+1} = 0$ . Taking  $-\epsilon^{n+1}$  as a test function in (3.21) yields:

$$\frac{1}{2} \|\epsilon^{n+1}\|_{L^2}^2 + \nu \delta t \|\nabla \epsilon^{n+1}\|_{L^2}^2 \leq C \delta t^2. \quad (3.21)$$

This end the proof.  $\square$

The spacial approximation error depends on the regularity of the solution  $\mathbf{v}$  and the approximation order of the scaling function basis. If the dual wavelet basis has  $r$  vanishing moments:

$$\int_{\mathbb{R}} x^k \tilde{\psi}(x) dx = 0, \quad 0 \leq k \leq r-1, \quad (3.22)$$

for all  $0 \leq s \leq r-1$ , the following Jackson type estimation holds:

$$\|\mathbf{v} - \mathbf{P}_j(\mathbf{v})\|_{L^2} \leq C 2^{-js} \|\mathbf{v}\|_{H^s(\Omega)}. \quad (3.23)$$

For edge scaling functions, the constant  $C$  in (3.23) is very important compared to internal scaling functions, this increases the numerical approximation error at the edges, which goes to zeros as  $j$  goes to infinity, see [24].

To investigate the convergence rates of the method, two numerical tests are conducted. The first one to evaluate the time discretization error and the second one to evaluate the spatial discretization error. As exact solution, we used:

$$\begin{cases} \mathbf{v}_1(x, y) = \cos(2\pi x) \sin(2\pi y) - \sin(2\pi y), \\ \mathbf{v}_2(x, y) = -\sin(2\pi x) \cos(2\pi y) + \sin(2\pi x), \\ p(x, y) = \cos(2\pi x) - \cos(2\pi y). \end{cases} \quad (3.24)$$

The right-hand side term  $\mathbf{f}$  is computed appropriately to ensure that (3.24) is the exact solution of (3.1) with  $\nu = 1/8\pi^2$ . The final time of the simulation is  $t = 10^{-2}$ , the maximal space resolution is fixed at  $j = 8$  and the wavelet generators of  $(V_j^1, \tilde{V}_j^1)$  correspond to biorthogonal spline with  $r = \tilde{r} = 3$ .

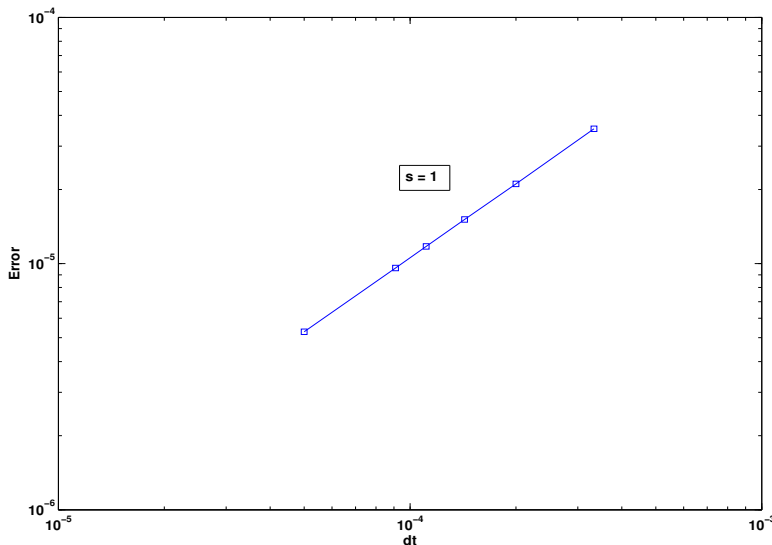


FIGURE 3.1. Time discretization  $\ell^2$ -error on  $\mathbf{v}$  according to the time step  $\delta t$ , log-log scale,  $j = 8$  and slope = 1.

REMARK 3.1.

*We notify that to achieve these experiences, all techniques on interpolation and extrapolation with biorthogonal multiresolution analyses on the interval  $[0, 1]$  must be well understood. We refer to [23, 24] for more details.*

Since the theoretical rate of convergence is obtained on Fig. 3.1, we investigate also the order of operator approximation (3.10) according to  $\nu t$  on a backward Euler scheme and on a Crank-Nicholson scheme. Fig. 3.2 shows this rate where the time step corresponds to  $\delta t = t/10$  in each case. For the spatial discretization error, the final time of the simulation is  $t = 10^{-4}$  and  $\delta t = t/10$ . Fig. (3.3) shows this error. Despite of the edge scaling functions approximation error effect, in the two cases, the expected rates of convergence are obtained.

### 3.2. Divergence-free Wavelet Schemes for Navier-Stokes Equations .

Divergence-free wavelet schemes in the numerical resolution of Navier-Stokes equa-

	$\ell^2$ -errors	$\nu t$	$\ell^2$ -errors	$\nu t$
Backward Euler	1.0446E <sup>-4</sup>	1.26.E <sup>-4</sup>	1.4620E <sup>-6</sup>	1.26E <sup>-6</sup>
Crank-Nicholson	2.8147E <sup>-5</sup>	-	4.9471E <sup>-8</sup>	-

FIGURE 3.2. Time discretization  $\ell^2$ -errors on  $\mathbf{v}$  according to  $\nu t$ .

Backward-Euler				
$j$	6	7	8	9
$L_2$ -error	1.9057E <sup>-4</sup>	1.6758E <sup>-5</sup>	1.46208E <sup>-6</sup>	7.1220E <sup>-7</sup>
$H^1$ -error	3.0627E <sup>-4</sup>	4.1319E <sup>-5</sup>	1.14088E <sup>-5</sup>	7.2127E <sup>-6</sup>
Crank-Nicholson				
$j$	6	7	8	9
$L_2$ -error	7.3498E <sup>-6</sup>	6.3924E <sup>-7</sup>	4.9471E <sup>-8</sup>	3.3322E <sup>-8</sup>
$H^1$ -error	1.0475E <sup>-4</sup>	9.5745E <sup>-6</sup>	1.410E <sup>-6</sup>	8.8480E <sup>-7</sup>

FIGURE 3.3. Spatial discretization  $\ell^2$ -errors according to the resolution  $j$ , for  $t = 10^{-4}$ .

tions were introduced firstly by Deriaz and Perrier [13, 14]. As mentioned in the introduction, the work of Deriaz and Perrier was limited to periodic boundary conditions. In this section, based on the projection method algorithms [7, 28], we are going to extend the works of [13, 14] to physical boundary conditions. This section gives also more details and precision on the step of projection of the method applied to Stokes equations in Section 3.1.

**3.3. Temporal discretization of Navier-Stokes equations.** In velocity pressure formulation, with physical boundary conditions, the most famous method in the numerical resolution of Navier-Stokes equations is the projection method [7, 28]. There is many kinds of projection method according to the chosen pressure boundary condition [1]. Without loss of generality, we focus here on the second order boundary approximation in time one, called projection method with accurate pressure boundary condition [15]. The principle steps of this method can be summarized as follows [15]:

- Prediction step: compute an intermediate velocity field  $\mathbf{v}^*$  such as

$$\begin{cases} \frac{\mathbf{v}^* - \mathbf{v}^n}{\delta t} + (\mathbf{v}^{n+1/2} \cdot \nabla) \mathbf{v}^{n+1/2} = \nu \Delta \frac{\mathbf{v}^* - \mathbf{v}^n}{2} \\ \mathbf{v}^* = 0, \text{ on } \partial\Omega \end{cases} \quad (3.25)$$

- Correction step: project  $\mathbf{v}^*$  onto the divergence-free functions space to get  $\mathbf{v}^{n+1}$

$$\begin{cases} \mathbf{v}^* = \mathbf{v}^{n+1} + \delta t \nabla p^{n+1/2}, \\ \nabla \cdot \mathbf{v}^{n+1} = 0, \\ \nabla p^{n+1/2} \cdot \mathbf{n} = -\mathbf{n} \cdot [\nabla \times (\nabla \times \mathbf{v}^*)], \text{ on } \partial\Omega \end{cases} \quad (3.26)$$

In the classical approaches [1, 7, 20, 28], to compute the velocity  $\mathbf{v}^{n+1}$ , one needs first to solve a Poisson equation:

$$\delta t \Delta p^{n+1/2} = \nabla \cdot \mathbf{v}^*, \quad (3.27)$$

and the specification of boundary for (3.27) defines the kind of projection operator. Otherwise, taking the inner product of the Navier-Stokes system (1.1) with the unit normal  $\mathbf{n}$  and unit tangent  $\mathbf{t}$  vectors at  $\partial\Omega$  leads respectively to

$$\nabla p \cdot \mathbf{n} = \nu \Delta \mathbf{v} \cdot \mathbf{n} \quad \text{and} \quad \nabla p \cdot \mathbf{t} = \nu \Delta \mathbf{v} \cdot \mathbf{t}. \quad (3.28)$$

Since the velocity  $\mathbf{v}^{n+1}$  is unknown in (3.26), boundary condition like (3.28) can not be incorporate directly to (3.27). To deal with this problem, several boundary conditions have been investigated in the literature [15, 20] and the most common one is:

$$\nabla p^{n+1/2} \cdot \mathbf{n} = 0. \quad (3.29)$$

Equation (3.29) defines an artificial Helmholtz decomposition of  $\mathbf{v}^*$ . This lack of appropriate boundary conditions for (3.26) is partly the reason of boundary's oscillation problem plaguing the projection method [15]. Particularly, the condition  $\nabla p^{n+1/2} \cdot \mathbf{n} = -\mathbf{n} \cdot [\nabla \times (\nabla \times \mathbf{v}^*)]$  is introduced to have  $O(\delta t^2)$  approximation order on  $\mathbf{v}^{n+1}$  at boundaries [15].

Since one knows to construct divergence-free wavelets basis satisfying boundary conditions, we are going to use this basis to compute the exact Helmholtz-Hodge decomposition of  $\mathbf{v}^*$  without using a Poisson equations solver. To this end, let us give some theoretical setting on the Helmholtz-Hodge decomposition in  $(H_0^1(\Omega))^d$ . Helmholtz-Hodge decomposition in  $(H_0^1(\Omega))^d$  is written slightly different, depending on the scalar product considered. Let us define the following divergence-free function space:

$$\mathcal{H}_{div,0}(\Omega) = \{\mathbf{u} \in (H_0^1(\Omega))^d : \nabla \cdot \mathbf{u} = 0\}. \quad (3.30)$$

The space  $\mathcal{H}_{div,0}(\Omega)$  is a proper closed subspace of  $(H_0^1(\Omega))^d$ , so we have:

$$(H_0^1(\Omega))^d = \mathcal{H}_{div,0}(\Omega) \oplus \mathcal{H}_{div,0}(\Omega)^\perp.$$

If we consider the standard scalar product of  $(H_0^1(\Omega))^d$  defined by:  $(\mathbf{u}, \mathbf{v})_{(H_0^1(\Omega))^d} = (\nabla \mathbf{u}, \nabla \mathbf{v})_{(L^2(\Omega))^d}$ , it is easy to prove:

$$\mathcal{H}_{div,0}(\Omega)^\perp = \{(-\Delta)^{-1} \nabla q : q \in L^2(\Omega)\}, \quad (3.31)$$

where  $(-\Delta)^{-1}$  denotes the Green's operator related to Dirichlet's homogeneous problem for  $-\Delta$  operator, see [18]. Otherwise, with the  $(L^2(\Omega))^d$  scalar product and using a coarse version of De Rham's theorem [18], it is known that if  $\mathbf{f} \in (H^{-1}(\Omega))^d$  satisfies

$$\langle \mathbf{f}, \mathbf{u} \rangle_{(L^2(\Omega))^d} = 0, \quad \forall \mathbf{u} \in \mathcal{H}_{div,0}(\Omega),$$

then there exists  $p \in L^2(\Omega)$  such that:

$$\mathbf{f} = \nabla p.$$

Then every function  $\mathbf{u} \in (H_0^1(\Omega))^d$  can be decomposed as:

$$\mathbf{u} = \mathbf{u}_{div,0} + \nabla p, \quad (3.32)$$

with  $p \in H^1(\Omega)$  and  $\mathbf{u}_{div,0} \in \mathcal{H}_{div,0}(\Omega)$ . We state that the curl-free component  $\nabla p$  is unique. Indeed, for  $\mathbf{u} \in (H_0^1(\Omega))^d$ , there exists a unique  $\mathbf{u}_{div,0} \in \mathcal{H}_{div,0}(\Omega)$  and a unique  $q \in L^2(\Omega)$  such that:

$$\mathbf{u} = \mathbf{u}_{div,0} + (-\Delta)^{-1} \nabla q.$$

Let  $\phi_1 \in H_0^2(\Omega)$  and  $\phi_2 \in (H_0^1(\Omega))^d$  be respectively the solutions of

$$-\Delta\phi_1 = q \quad \text{and} \quad -\Delta\phi_2 = \nabla q.$$

By the uniqueness of these solutions, we get :  $\phi_2 = \nabla\phi_1 = (-\Delta)^{-1}\nabla q$ . Then,  $\mathcal{H}_{div,0}(\Omega)^\perp$  is a curl-free function space, derived from scalar potentials.

Decomposition (3.32) can not be computed with classical algorithm based on Poisson solver. Taking the inner product of (3.32) with the unit normal  $\mathbf{n}$  and unit tangent  $\mathbf{t}$  vectors respectively yields:

$$\nabla p \cdot \mathbf{n} = 0 \quad \text{and} \quad \nabla p \cdot \mathbf{t} = 0, \quad (3.33)$$

and satisfying both these boundary conditions on  $p$  is very difficult in practice. Thus, system (3.26) is not a Helmholtz-Hodge decomposition, as far as that goes for (3.26) with only boundary condition (3.29). Further, setting  $\mathbf{v}^* = \mathbf{v}^{n+1} + \delta t \nabla p^{n+1/2}$  with both  $\mathbf{v}^*$  and  $\mathbf{v}^{n+1}$  in  $(H_0^1(\Omega))^d$  leads necessarily to boundary conditions (3.26) on the pressure  $p^{n+1/2}$ . Moreover, up to an integration constant, each boundary condition in (3.33) defines a unique solution  $p^{n+1/2}$  to (3.27), what makes more difficult the numerical resolution.

Analysing differently the problem and trusting the Poisson equations solver, one can take advantage of the boundary conditions like (3.33) and the Helmholtz-Hodge decomposition to derive new correction step for (3.25). Indeed, let  $\phi^{n+1/2}$  be a scalar potential in  $L^2(\Omega)$  satisfying

$$\tilde{\mathbf{v}} = \mathbf{v}^{n+1} + \delta t \nabla \phi^{n+1/2}, \quad \text{with} \quad \tilde{\mathbf{v}} \in (H_0^1(\Omega))^d. \quad (3.34)$$

Substituting this change of variable in (3.25), it comes that the vector function  $\tilde{\mathbf{v}}$  verifies the system

$$\begin{cases} \frac{\tilde{\mathbf{v}} - \mathbf{v}^n}{\delta t} + (\mathbf{v}^{n+1/2} \cdot \nabla) \mathbf{v}^{n+1/2} = \nu \Delta \frac{\tilde{\mathbf{v}} - \mathbf{v}^n}{2} \\ \tilde{\mathbf{v}} = 0, \quad \text{on} \quad \partial\Omega \end{cases} \quad (3.35)$$

and the new correction step is defined by:

$$\mathbf{v}^{n+1} = \mathbb{P}(\tilde{\mathbf{v}}), \quad (3.36)$$

where  $\mathbb{P}$  denotes the orthogonal projector from  $(H_0^1(\Omega))^d$  onto  $\mathcal{H}_{div,0}(\Omega)$ , according to the  $(L^2(\Omega))^d$  scalar product. As the same, the pressure  $p^{n+1/2}$  is uniquely defined up to a constant from  $\phi^{n+1/2}$  by:

$$p^{n+1/2} = \phi^{n+1/2} - \frac{\nu \delta t}{2} \Delta \phi^{n+1/2}. \quad (3.37)$$

In the same way, according to (3.31), if we replace  $\nabla \phi^{n+1/2}$  by  $(-\Delta)^{-1} \nabla \phi^{n+1/2}$  in (3.34), we can define  $p^{n+1/2}$  by:

$$\nabla p^{n+1/2} = (-\Delta)^{-1} \nabla \phi^{n+1/2} + \frac{\nu \delta t}{2} \nabla \phi^{n+1/2}, \quad (3.38)$$

In each two cases, Navier-Stokes formulation (3.35) is a change of variables and this is a great difference from the classical projection methods which are operator's splitting.

#### REMARK 3.2.

Equation (3.38) is a classical Helmholtz equation with Dirichlet homogeneous boundary condition, for the unknown  $(-\Delta)^{-1} \nabla \phi^{n+1/2}$ .

**3.4. Spatial discretization.** The spatial discretization we use is the same as for the Stokes equations in Section 3.1. Then, at a given resolution  $j$ , the components of  $\mathbf{v}^n$  are searched in the form of a finite dimensional wavelet basis series:

$$\mathbf{v}_1^n = \sum_{|\mathbf{j}| < j, \mathbf{k}} d_{\mathbf{j}, \mathbf{k}}^{1,n} \psi_{j_1, k_1}^1 \otimes \psi_{j_2, k_2}^0 \quad \text{and} \quad \mathbf{v}_2^n = \sum_{|\mathbf{j}| < j, \mathbf{k}} d_{\mathbf{j}, \mathbf{k}}^{2,n} \psi_{j_1, k_1}^0 \otimes \psi_{j_2, k_2}^1, \quad (3.39)$$

and similarly for  $\tilde{\mathbf{v}}$  with coefficients  $[\tilde{d}_{\mathbf{j}, \mathbf{k}}^1]$  and  $[\tilde{d}_{\mathbf{j}, \mathbf{k}}^2]$ . Following [1, 20], the nonlinear term  $(\mathbf{v}^{n+1/2} \cdot \nabla) \mathbf{v}^{n+1/2}$  is approximated by:

$$(\mathbf{v}^{n+1/2} \cdot \nabla) \mathbf{v}^{n+1/2} = \frac{3}{2} (\mathbf{v}^n \cdot \nabla) \mathbf{v}^n - \frac{1}{2} (\mathbf{v}^{n-1} \cdot \nabla) \mathbf{v}^{n-1}, \quad (3.40)$$

and (3.40) is computed explicitly with finite differences method on the mesh grid points. Next, each component of  $(\mathbf{v}^{n+1/2} \cdot \nabla) \mathbf{v}^{n+1/2}$  is projected respectively onto the wavelets basis  $\{\psi_{j_1, k_1}^1 \otimes \psi_{j_2, k_2}^0\}$  and  $\{\psi_{j_1, k_1}^0 \otimes \psi_{j_2, k_2}^1\}$ . This choice impose a CFL condition on the time step [13]:  $\delta t \leq C \delta x^{4/3}$ .

The computation of coefficients  $[\tilde{d}_{\mathbf{j}, \mathbf{k}}^1]$  and  $[\tilde{d}_{\mathbf{j}, \mathbf{k}}^2]$  from those of  $\mathbf{v}^n$  and  $(\mathbf{v}^{n+1/2} \cdot \nabla) \mathbf{v}^{n+1/2}$ , is reduced to solving a matrices linear system:

$$\mathcal{A}_{\frac{\delta t}{2}}^1 [\tilde{d}_{\mathbf{j}, \mathbf{k}}^1] \mathcal{A}_{\frac{\delta t}{2}}^0 = \mathcal{R}_{\frac{\delta t}{2}}^1 [d_{\mathbf{j}, \mathbf{k}}^{1,n}] \mathcal{R}_{\frac{\delta t}{2}}^0 - \delta t \mathcal{M}^1 [(\mathbf{v}^{n+1/2} \cdot \nabla) \mathbf{v}^{n+1/2}]_1 \mathcal{M}^0, \quad (3.41)$$

$$\mathcal{A}_{\frac{\delta t}{2}}^0 [\tilde{d}_{\mathbf{j}, \mathbf{k}}^2] \mathcal{A}_{\frac{\delta t}{2}}^1 = \mathcal{R}_{\frac{\delta t}{2}}^0 [d_{\mathbf{j}, \mathbf{k}}^{2,n}] \mathcal{R}_{\frac{\delta t}{2}}^1 - \delta t \mathcal{M}^0 [(\mathbf{v}^{n+1/2} \cdot \nabla) \mathbf{v}^{n+1/2}]_2 \mathcal{M}^1, \quad (3.42)$$

where  $\mathcal{M}^\epsilon$ ,  $\mathcal{A}_{\frac{\delta t}{2}}^\epsilon$  and  $\mathcal{R}_{\frac{\delta t}{2}}^\epsilon$  correspond to mass matrices and stiffness matrices of operators  $(1 - \frac{1}{2} \delta t \nu \Delta)$  and  $(1 + \frac{1}{2} \delta t \nu \Delta)$  on the one-dimensional bases of  $\{V_j^\epsilon\}_{\epsilon=0,1}$  respectively.

**4. Lid driven cavity flow.** To validate the divergence-free wavelet modified projection method, in the case of Navier-Stokes equations, we focus on the classical problem of lid-driven cavity flow. This problem has been investigate by many authors since the pioneer work of [3, 17]. Recently, Bruneau and Saad [4] have revised this problem and obtained good results using multigrid solver with various and special numerical discretization technique. The particularity of the work of [4] resides in the special discretization of the convection term and high space resolution are used:  $j = 10$  or  $j = 11$ .

The objective in this section is to compare the results obtains with method (3.35) and (3.36) to those of [3, 4, 17]. Thus, one can evaluate the accuracy and performance of this new method. The wavelet basis generators of  $(V_j^1, \tilde{V}_j^1)$  are the biorthogonal spline with three vanishing moments:  $r = \tilde{r} = 3$ . Since the horizontal velocity  $\mathbf{v}_1$  does not satisfy homogeneous Dirichlet boundary condition, homogenization technique is used for this component [24]. The advection term  $(\mathbf{v}^n \cdot \nabla) \mathbf{v}^n$  is computed with a tow-order finite difference method on the mesh grid points. On Fig. 4.1 and Fig. 4.2, we plot the middle horizontal and vertical profiles of the velocity obtained for  $j = 7$  and  $Re = 1000$ , compared to the results of [4] obtained with  $j = 10$ . Fig. 4.3 and Fig. 4.4, show the values of these profiles for  $j = 7$  and  $j = 8$ , compared to the results of the work of literature.

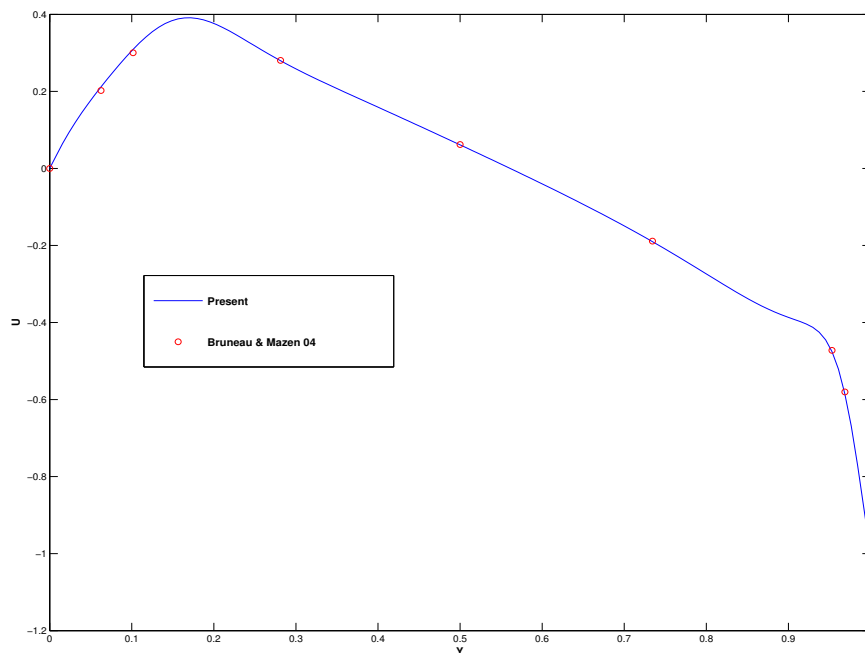


FIGURE 4.1. Horizontal velocity profile  $v_1$  in the middle of the cavity at the steady state. Solid line (present work) and circle (Bruneau et Saad [4]):  $Re = 1000$  and  $j = 7$ .

#### REFERENCES

- [1] J. B. BELL, P. COLELLA, H. M. GLAZ, *A second-order projection method for the incompressible Navier-Stokes equations*, J. Comput. Phys., 85 (1989) pp. 257–283.
- [2] G. BEYLKIN, *On the representation of operator in bases of compactly supported wavelets*, SIAM J. Numer. Anal., 6 (1992), pp. 1716–1740.
- [3] O. BOTELLA, R. PEYRET, *Benchmark spectral results on the lid-driven cavity flow*, Comput. Fluids, 27 (1998), pp. 421–433.
- [4] C.-H. BRUNEAU, M. SAAD, *The 2D lid-driven cavity problem revised*, Comput. Fluids, 35 (2006), pp. 326–348.
- [5] C. CANUTO, R. MASSON, *Stabilized wavelet approximations of the Stokes problem*, Math. of Comp., 70 (2001), pp. 1397–1416.
- [6] P. CHARTON, V. PERRIER, *A Pseudo-Wavelet Scheme for the Two-Dimensional Navier-Stokes Equations*, Comp. Appl. Math., 15 (1996), pp. 137–157.
- [7] A.J. CHORIN, *Numerical simulation of the Navier-Stokes equation*, Math. Comp., 22 (1968), pp. 745–762.
- [8] A. COHEN, *Numerical Analysis of Wavelet Methods*, Elsevier, 2003.
- [9] A. COHEN, I. DAUBECHIES, J.-C. FEAUVEAU, *Biorthogonal bases of compactly supported wavelets*, Comm. Pure Appl. Maths., 45 (1992), pp. 485–560.
- [10] A. COHEN, I. DAUBECHIES, P. VIAL, *Wavelets on the Interval and Fast Wavelet Transforms*, Appl. Comput. Harmon. Anal., 1 (1993), pp. 54–81.
- [11] W. DAHMEN, K. URBAN, J. VORLOEPER, *Adaptive Wavelet Methods-Basic Concepts and Appli-*



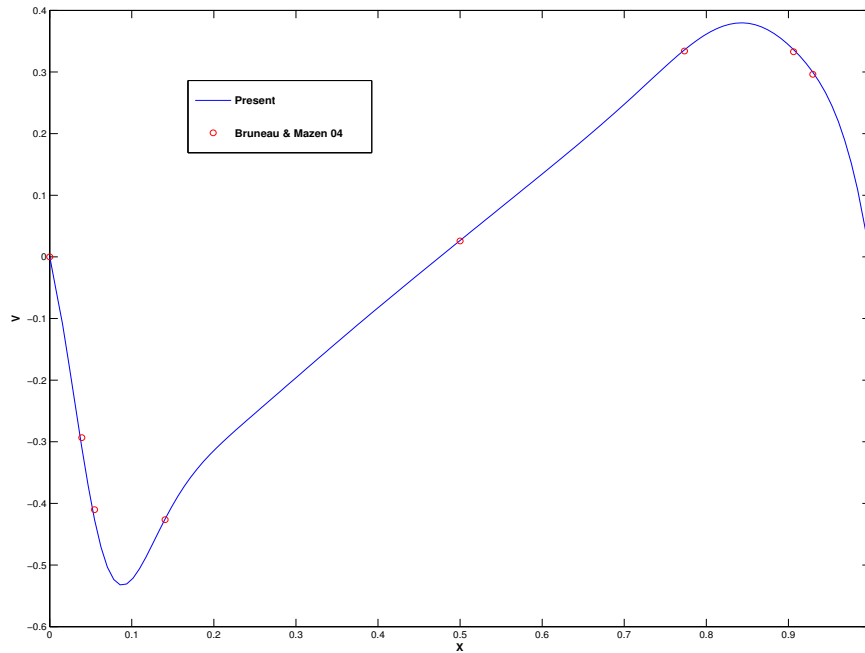


FIGURE 4.2. Vertical velocity profile  $\mathbf{v}_2$  in the middle of the cavity at the steady state. Solid line (present work) and circle (Bruneau et Saad [4]):  $Re = 1000$  and  $j = 7$ .

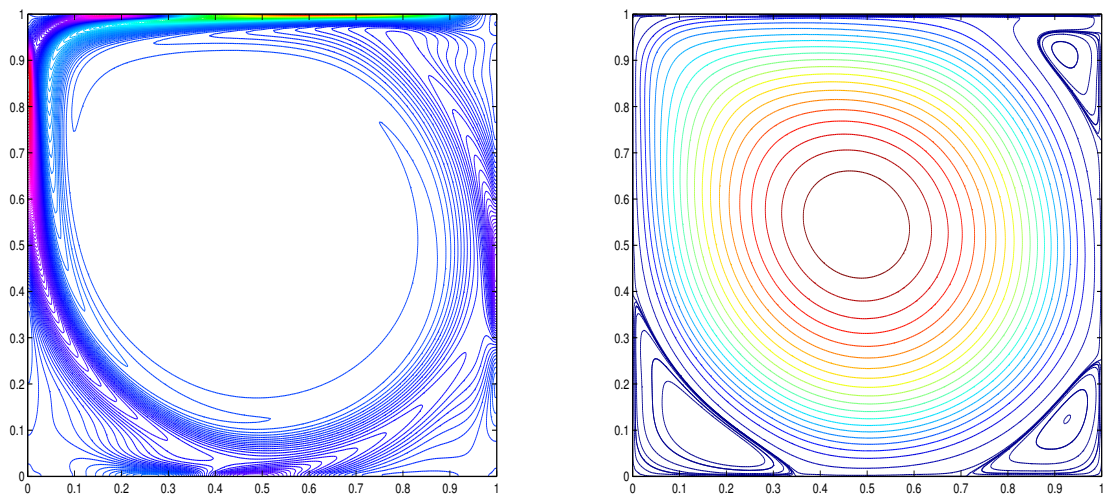
$y$	$\mathbf{v}_1$ , Present $j = 7$	$\mathbf{v}_1$ , Present $j = 8$	$\mathbf{v}_1$ , Ref. [3]	$\mathbf{v}_1$ , Ref. [4]	$\mathbf{v}_1$ , Ref. [17]
1	-1.0000	-1.0000	-1.0000	-1.0000	-1.0000
0.9688	-0.5850	-0.5809	-0.5808	-0.5803	-0.5749
0.9531	-0.4756	-0.4726	-0.4723	-0.4723	-0.4660
0.7344	-0.1901	-0.1887	-0.1886	-0.1886	-0.1871
0.5000	0.0618	0.0617	0.0620	0.0620	0.0608
0.2813	0.2797	0.2800	0.2803	0.2804	0.2780
0.1016	0.3091	0.3020	0.3004	0.3002	0.2973
0.0625	0.2116	0.2013	0.2023	0.2022	0.2019
0.0000	0.0000	0.0000	0.0000	0.0000	0.0000

FIGURE 4.3. Spatial errors according to the resolution  $j$ , for  $t = 10^{-4}$ .

*cations to the Stokes Problem, Wavelet Analysis—Twenty Years Developments*, Ding-Xuan Zhou ed., World Scientific, New Jersey, (2002), pp. 39–80.

- [12] E. DERIAZ, V. PERRIER, *Orthogonal Helmholtz decomposition in arbitrary dimension using divergence-free and curl-free wavelets*, Appl. Comput. Harmon. Anal., 26 (2009), pp. 249–269.
- [13] E. DERIAZ, V. PERRIER, *Direct Numerical Simulation of Turbulence using divergence-free wavelets*, SIAM Multis. Model. and Simul., 7 (2008), pp. 1101–1129.
- [14] E. DERIAZ, V. PERRIER, *Divergence-free and curl-free wavelets in 2D and 3D, application to turbulent flows*, J. of Turbulence, 7 (2006), pp. 1–37.
- [15] W. E, J. GUO-LIU, *Projection Method I: Convergence and Numerical Boundary Layers*, SIAM

$x$	$\mathbf{v}_2$ , Present $j = 7$	$\mathbf{v}_2$ , Present $j = 8$	$\mathbf{v}_2$ , Ref. [3]	$\mathbf{v}_2$ , Ref. [4]	$\mathbf{v}_2$ , Ref. [17]
0.0000	0.0000	0.0000	0.0000	0.0000	0.0000
0.0391	-0.3086	-0.2968	-0.2936	-0.2933	-0.2766
0.0547	-0.4267	-0.4137	-0.4103	-0.4101	-0.3918
0.1406	-0.4253	-0.4257	-0.4264	-0.4263	-0.4266
0.5000	0.0266	0.0259	0.0257	0.0258	0.0252
0.7734	0.3359	0.3340	0.2803	0.2804	0.2780
0.9062	0.3364	0.3333	0.3339	0.3339	0.3307
0.9297	0.2998	0.2967	0.2962	0.2962	0.2901
1.0000	0.0000	0.0000	0.0000	0.0000	0.0000

FIGURE 4.4. Spatial errors according to the resolution  $j$ , for  $t = 10^{-4}$ .FIGURE 4.5. Vorticity contour (left) and divergence-free scaling function coefficients contour (right),  $Re = 2000$  and  $j = 8$ .

- J. Numer. Anal., 32 (1995), pp. 1017–1057.
- [16] J. FROHLICH, K. SCHNEIDER, *Numerical Simulation of Decaying Turbulence in an Adaptive Wavelet Basis*, Appl. Comput. Harm. Anal, 3 (1996), pp. 393–397.
- [17] U.GHIA, K. N. GHIA, C. T. SHIN, *High-Re solutions for incompressible flows using Navier-Stokes equations and a multigrid method*, J. Comput. Phys., 48 (1982), pp. 387–411.
- [18] V. GIRAULT, P.A. RAVIART, *Finite element methods for Navier-Stokes equations*, Springer-Verlag Berlin, 1986.
- [19] A. JOUINI, P.G. LEMARIÉ-RIEUSSET, *Analyse multirésolution biorthogonale sur l'intervalle et applications*, Annales de l'I.H.P. Section C, 10 (1993), pp. 453–476.
- [20] J. KIM, P. MOIN, *Application of a fractional-step method to incompressible Navier-Stokes equations*, J. Comp. Phys., 59 (1985), pp. 308–323.
- [21] P. G. LEMARIÉ-RIEUSSET, *Analyses multi-résolutions non orthogonales, commutation entre projecteurs et dérivation et ondelettes vecteurs à divergence nulle*, Revista Matemática Iberoamericana, 8 (1992), pp. 221–236.
- [22] J.-G. LIU, J. LIU, R. PEGO, *Stable and accurate pressure approximation for unsteady incompressible viscous flow*, J. Comput. Phys., 229 (2010), pp. 3428–3453.
- [23] P. MONASSE, V. PERRIER, *Orthogonal Wavelet Bases Adapted For Partial Differential Equations With Boundary Conditions*, SIAM J. Math. Anal., 29 (1998), pp. 1040–1065.

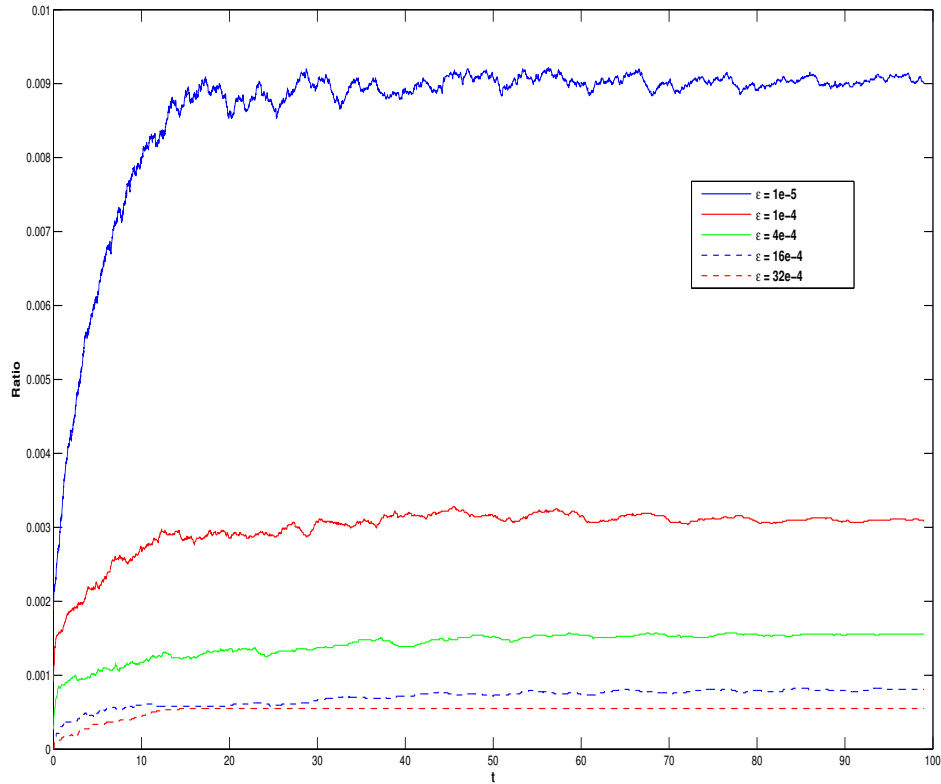


FIGURE 4.6. Evolution of the ratio of divergence-free wavelet coefficients up to a fixed  $\epsilon$ .

- [24] K.-H. SOULEYMANE, *Ondelettes pour la prise en compte de conditions aux limites en turbulence incompressible*, Phd thesis, Grenoble University, 2010.
- [25] K.-H. SOULEYMANE, V. PERRIER, *Helmholtz-Hodge Decomposition on  $[0, 1]^d$  by Divergence-free and Curl-free Wavelets*, accepted for publication, proceedings curves and surfaces conf., Springer Lecture Notes in Computer Science (2011) .
- [26] K.-H. SOULEYMANE, V. PERRIER, *Divergence-free and curl-free wavelets on the square for numerical simulations*, Grenoble University, preprint submitted (2011) .
- [27] R. STEVENSON, *Divergence-free wavelet bases on the hypercube: Free-slip boundary conditions, and applications for solving the instationnary Stokes equations*, Math. Comp. 80 (2011), pp. 1499–1523.
- [28] R. TEMAM, *Sur l'approximation de la solution des équations de Navier-Stokes par la méthode des pas fractionnaires II*, Arch. Rational Mech. Anal. 33 (1969), pp. 377–385.
- [29] R. TEMAM, *Navier Stokes Equations*, North Holland, New York, 1977.
- [30] K. URBAN, *Using divergence-free wavelets for the numerical solution of the Stokes problem*, AMLF'96: Proceedings of the Conference on Algebraic Multilevel Iteration Methods with Applications University of Nijmegen, The Netherlands, 2 (1996), pp. 261–277.
- [31] K. URBAN, *Wavelets in Numerical Simulation*, Springer Berlin, 2002.
- [32] C. WANG, J-G. LIU, *Convergence of Gauge method for incompressible flow*, Math. Comput., 69 (2000), pp. 1385–1407.

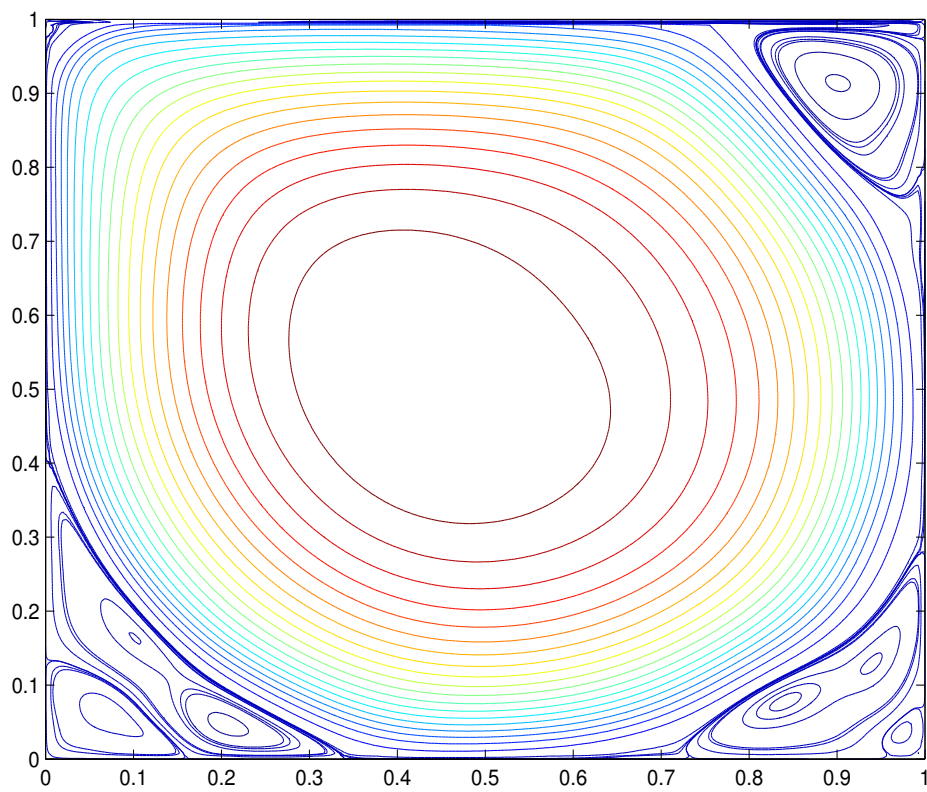


FIGURE 4.7. *Divergence-free scaling function coefficients contour at  $t = 80$ ,  $Re = 10000$  and  $j = 8$ .*

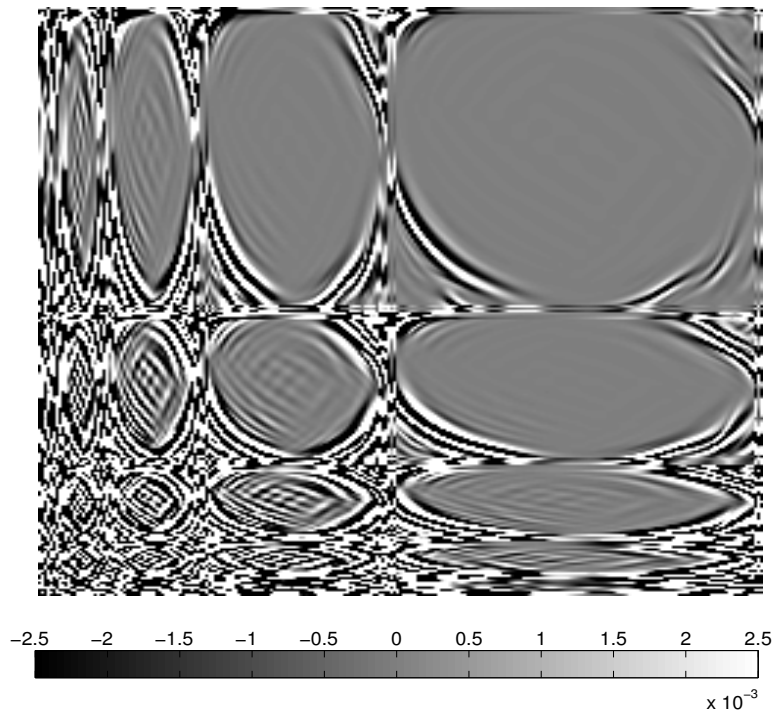


FIGURE 4.8. *Divergence-free scaling function coefficients contour at  $t = 80$ ,  $Re = 10000$  and  $j = 8$ .*